HIGH RESOLUTION DISTRIBUTED TEMPERATURE MEASUREMENTS USING OPTICAL FIBERS IN A MOLTEN SALT FORCED CONVECTION ENVIRONMENT

A Thesis

by

BLAIN R. LANCASTER

Submitted to the Office of Graduate and Professional Studies of
Texas A&M University
in partial fulfillment of the requirements for the degree of

MASTER OF SCIENCE

Chair of Committee,	Yassin Hassan
Committee Members,	Rodolfo Vaghetto
	Lesley Wright
Head of Department,	Bryan Rasmussen

May 2021

Major Subject: Mechanical Engineering

ABSTRACT

The high temperatures and corrosive environment created by molten salts pose challenges to both traditional and advanced measurement techniques. Experimental measurements of thermal-hydraulic parameters in these environments are paramount to advance the understanding of the molten salts' behavior, and are necessary for future validation of computational models. An experimental test facility is utilized to characterize the thermal-hydraulic behavior of typical molten salts under steady-state and transient, forced flow conditions, by employing innovative measurement methods. Optical Fiber Distributed Temperature Sensors (OFDTS) have the ability to provide high resolution temperature measurements. These sensors capacity to provide temperature profiles are useful as a monitoring system, and for validation with simulations. Through this experimental study, the application of this technology has been extended to high temperature forced convection environments using FLiNaK as an operating fluid. Axial and radial temperature distributions have been recorded, and two-dimensional temperature fields have been reconstructed from the OFDTS network installed in this facility. Molten salt front velocity has been estimated from this. The effect of OFDTS external coating type, as well as installation configuration was investigated as well. The coatings tested are Polyimide, Aluminum, and a Gold-Carbon hybrid. The different coated OFDTS are specified to have different operating ranges, all below the 600°C temperature of this facility. However, this is a parameter that is based on the coating itself, not the ability of a fiber to make successful measurements. By examining response times and success of these different sensors for their duration under high temperatures, it was concluded that these coatings have little effect on response time or durability. In addition to this, shorter segments as seen in the radial installations see more longevity compared to longer (axial) segments under the same amount of time at temperatures above 500°C. Based on this, it is recommended that polyimide fibers be used even at these high temperatures, due to being the least expensive of the three tested, as well as being the easiest to fabricate into a sensor. Shorter segments exposed too high temperature (< 0.4 m) are also recommended due to the repeated failure of the axial OFDTS.

ACKNOWLEDGMENTS

I would like to thank Dr. Yassin Hassan and Dr. Rodolfo Vaghetto for having me on this project and making my graduate school lab experience the best it could be. Thank you to Dr. Lesley Wright for taking the time to serve on my committee.

Thank you to the students who began work on this facility long before I arrived at the lab, especially Ojasvin Arora who I have worked with since I arrived. Thanks and credit to Will Headley, Dr. Sero Yang and numerous undergraduates as well.

CONTRIBUTORS AND FUNDING SOURCES

Contributors

This work was supported by a thesis committee consisting of Dr. Yassin Hassan (advisor) of the Department of Mechanical Engineering, Dr. Rodolfo Vaghetto of the Department of Nuclear Engineering, and Dr. Lesley Wright of the Department of Mechanical Engineering

Funding Sources

This study was supported by funding provided by the Thorium Research Initiative.

NOMENCLATURE

MS	Molten Salts
CSP	Concentrated Solar Power
MSR	Molten Salt Reactor
LWR	Light Water Reactors
FHR	Fluoride-Salt-Cooled High-Temperature Reactor
LFTR	Liquid Fluoride Thorium Reactor
ORNL	Oak Ridge National Laboratory
OFS	Optical Fiber Sensor
DTS	Distributed Temperature Sensing
OFDTS	Optical Fiber Distributed Temperature Sensing
FLiNaK	Eutectic salt mixture of LiF-NaF-KF
SS316	Stainless-Steel 316
PLC	Programmable Logic Controller
OPC	Open Platform Communications
DAQ	Data Acquisition system
ODiSI	Optical Distributed Sensor Interrogator
DAQ	Data Acquisition system
NA	Numerical Aperture
OFDR	Optical Frequency Domain Reflectometry
SM	Single Mode fiber
PTFE	Polytetrafluoroethylene
RTD	Resistance Temperature Detector
σ_X	Uncertainty from source X

TABLE OF CONTENTS

Page

LIST OF FIGURES

FIGURE Page

LIST OF TABLES

TABLE Page

1. INTRODUCTION

Molten salts (MS) have become a widely researched fluid for many applications involving energy storage and heat transfer. Their unique characteristics such as high heat capacity and operability at moderate to high temperatures makes them ideal for these applications [1], especially in regards to alternative energy solutions. Concentrated Solar Power (CSP) and Molten Salt Reactor (MSR) technologies are both making strides to utilize fluoride salt mixtures for heat storage as well as coolants. MSRs aim to provide cleaner, more efficient nuclear energy by offering advantages over typical Light Water Reactors (LWR) such as their numerous configurations and categorizations. Fluoride High Temperature Reactors (FHR) utilize molten salts as a coolant only, while maintaining solid nuclear fuel. The Liquid Fluoride Thorium Reactor (LFTR) is a type of MSR that uses a thorium based molten fluoride salt as a fuel, which transfers heat to a secondary, non-radioactive salt [2]. This concept was first investigated by Oak Ridge National Laboratory (ORNL) in the 1960's, but used Uranium-233 and 235 rather than thorium. Though their experiments proved that this concept of the LFTR is viable, it revealed a need for further understanding of thermal-hydraulic and physical properties of liquid fluoride salts. Currently, research revolves around design and optimization of systems for use with molten salts. This also extends to the development and implementation of new sensors and measurement techniques. There is also a lack of experimental data needed to validate thermal-hydraulic computational models with molten salts [3]. Due to high operating temperatures and the corrosive nature of molten salts, non-intrusive techniques such as ultrasonic flow meters are being considered but have not yet been successfully used in this environment [4]. More sophisticated measurement techniques are also being explored for use in industrial and nuclear applications, as is the case with Optical Fiber Sensors (OFS). Due to their high sensitivity, and ability to be used as Distributed Temperature Sensing (DTS) devices, OFS are being considered as a monitoring system for the variables in nuclear plants [5]. These sensors are able to achieve high spatial resolutions but face challenges when used in a forced flow molten salt environment such as exposure to high temperatures and corrosive environments, flow

induced vibrations, mechanical, and thermal stresses. The technology of OFS as a distributed temperature sensing device has been proven in low temperature environments [6, 7], but successful use in the higher operating temperatures such as those found in the extreme environments of MSRs requires further investigation. In order to replicate such environments, a small scale test facility has been constructed to perform forced flow experiments with molten salts in order to demonstrate the feasibility of molten salt reactor technologies, as well as provide validation for the instrumentation used. Current published works regarding molten salts focus on establishing their thermophysical properties as a function of temperature, [8, 9, 10], while others aimed to study the thermal-hydraulic behaviors of different salts under various operating conditions. Britsch et al. [11] and Srivastava et al. [12] have performed investigations on natural circulation of molten salts, and Bin et al. [13] and Wu et al. [14] have investigated their turbulence and heat transfer under forced convection.

2. OBJECTIVE

The purpose of this research is to explore, test, and deploy advanced temperature measurement techniques in molten salt environments, to produce high fidelity - high spatial resolution temperature profiles. These profiles can be used not only to better understand the flow behavior under steady and transient conditions, but to provide information of the front transition velocity, and contribute to the future validation of advanced computational tools. The goals for the test facility were devised as follows:

- Prepare a test environment to conduct OFDTS measurements (test setup, identify best installation techniques etc.)
- Perform tests to identify the most suitable fiber technology to be deployed to these systems
- Conduct temperature measurements, and study flow behavior (supported by other thermal-hydraulic measurements)

Overall this study aims to fill the gap of available experimental data of molten salt thermal-hydraulic behavior, especially that of high temperature OFS measurements, in a forced convection environment. The fluid of interest for this project is FLiNaK, a eutectic mixture of Lithium Fluoride, Sodium Fluoride and Potassium Fluoride, which has a melting point of 454°C. The FLiNaK is to be heated to a temperature well above its melting point and pumped through a stainless-steel pipe in a loop configuration. The test loop contains instrumentation for measuring pressure, flow rate, and temperature with thermocouples and OFS. With limited documentation regarding the use of OFS in these environments, this research is important to confirm OFS success in regard to signal quality, installation methods, as well as types of fibers and coatings by observation of resulting temperature profiles. The repeatability of measurements with OFS is dependent on the integrity of the fiber following operation at high temperatures. Thus, the success and consistent operation of these sensors is evaluated with multiple tests.

3. EXPERIMENTAL FACILITY OVERVIEW

An existing experimental facility in operation at the Texas A&M University Thermal Hydraulics Research Laboratory was outfitted with an updated test section and instrumentation for the purposes of this research. This facility, with its features and capabilities are described in detail in the next subsection.

3.1 Tank and Pump Design

The test facility utilized in this study is a closed loop system constructed for the purposes of operating at high temperatures of up to 700°C. This operating range was chosen specifically with the goal of forced flow operation with molten salts in mind. The facility includes a centrifugal, high-temperature pump, a sump tank with electric heating elements, and the test loop. The pump has a flow operating range of 0 to 150 lpm. The pump is mounted to the tank via a large flange with multiple access ports leading to the sump tank. These ports are utilized for pouring the powdered salt into the tank, measuring salt temperature with a thermocouple probe, and for argon gas inlet and outlet. There are also two ports that act as the inlet and outlet for the molten salt as it flows between the sump tank and the test loop. The inlet port is connected to a pipe inside the sump tank that leads to a casing surrounding the impeller. The impeller casing pulls molten salt from an opening in the bottom, pumping directly to the inlet port. A stainless-steel flanged elbow is welded to the inlet and outlet ports, which act as the connection points for the test loop. The sump tank has the capability to hold a total of 28 liters of fluid. As mentioned previously, the tank also has independent heaters wrapped around it and below it. Each heater's power is controlled by setting a desired temperature via a Programmable Logic Controller (PLC) with the thermocouple probe as the reference for the top heater, while the bottom heater has an embedded temperature sensor. An overview of the whole facility is shown in figure 3.1.

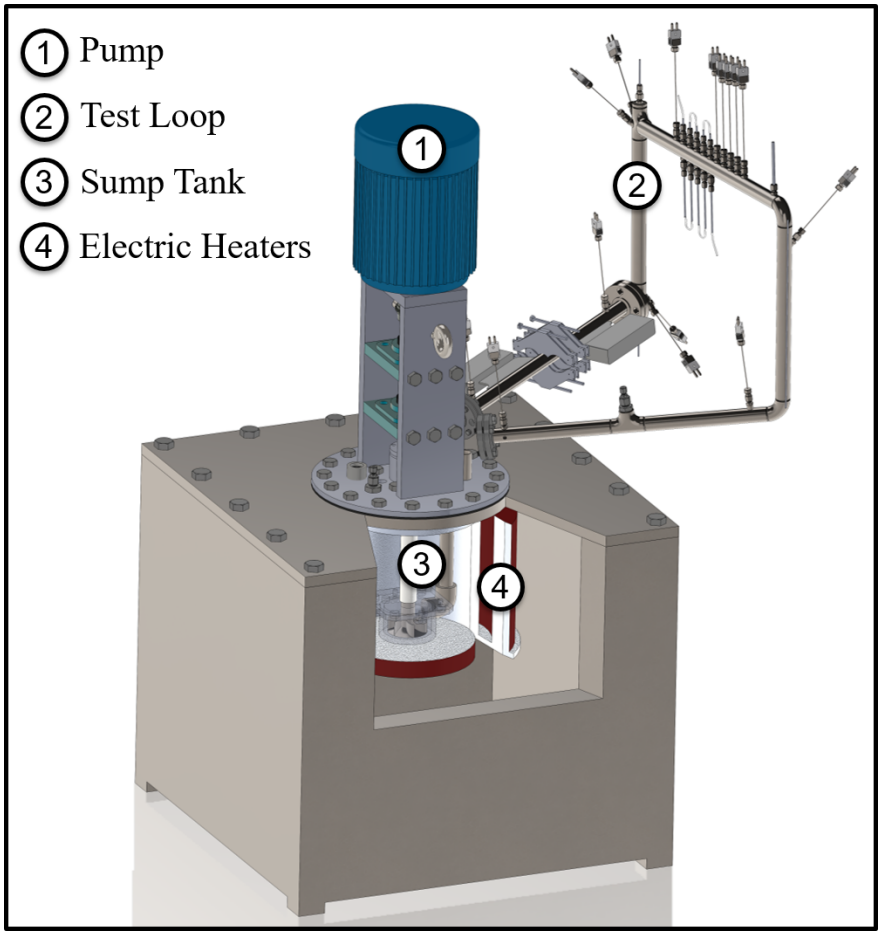

Figure 3.1: Schematic representation of the molten salt test facility.[15]

3.2 Test Loop Design

The test loop is a 1" schedule 40 pipe and consists of five major segments, which may be referred to as "legs" in this document. All components of the system in direct contact with the liquid salt, including test loop, pump components and sump tank, are made out of stainless steel Type 316L and are thermally insulated on portions exposed to the ambient air. SS316 was chosen for its resistance to corrosion, and ability to operate in high temperature environments with many thermal cycles. The test loop is designed with legs 1, 3, and 5 as horizontal sections, and legs 2 and 4 as vertical sections. This shape combined with an 8° inclination angle of the horizontal sections allows for the salt to flow from the loop and back into the sump tank upon completion

of a test, minimizing salt solidification in the loop. The shape also allows for sufficient length of pipe to accommodate all the instrumentation, while occupying only a small physical space. As mentioned there are flanges at the inlet and outlet of the loop to connect to the elbows leading to the sump tank. Legs 1 and 2 also connect via a flange. This was done to keep leg 1 removable due to machining considerations, in which flat faces are needed on the sides for the selected flow meter. In order to ensure a leak proof seal at the flange interfaces, a Vermiculite gasket is used. These are spiral wound gaskets that utilize Thermiculite® 835 as the filler material and SS316 as the outer ring. These gaskets were selected for their operability at extreme temperature ranges in addition to corrosion resistance.

In order to compensate for heat losses, the loop temperature must be controlled before pumping of the salt. To do this electric tracer heaters in the from of heating tapes are wrapped around each leg. The test loop is outfitted with various instrumentation along each leg of the test loop to evaluate the system-level thermal hydraulics of this forced convection environment. The flow rate, and pressure drop are measured, as well as fluid and wall temperatures with thermocouples and Optical Fiber Distributed Temperature Sensors (OFDTS), with the goal of characterizing the temperature profiles of the salt under steady-state and transient conditions. A detailed view of the test loop is shown in figure 3.2.

Various different flow measurement devices have been considered for this loop. Among the techniques investigated, the ultrasonic flow meter technology provides a means to operate non-intrusively with a variety of different fluids. This non-intrusive method removes the flow devices contact with the salt, potentially increasing the lifetime of the measuring device and lowering maintenance needs. Based on a similar need, a differential pressure sensor was chosen that avoids direct contact between delicate components and the molten salt. This sensor contains two transducers that utilize a stainless-steel diaphragm interfacing with the salt. The transducers are attached to a sodium-potassium (NaK) filled transfer line, that connects to the transmitter, preventing it from coming in direct contact with the salt. As shown in figure 3.2, leg 1 contains a high temperature ultrasonic flow meter by FLEXIM® as well as a port for the high pressure side of the differential

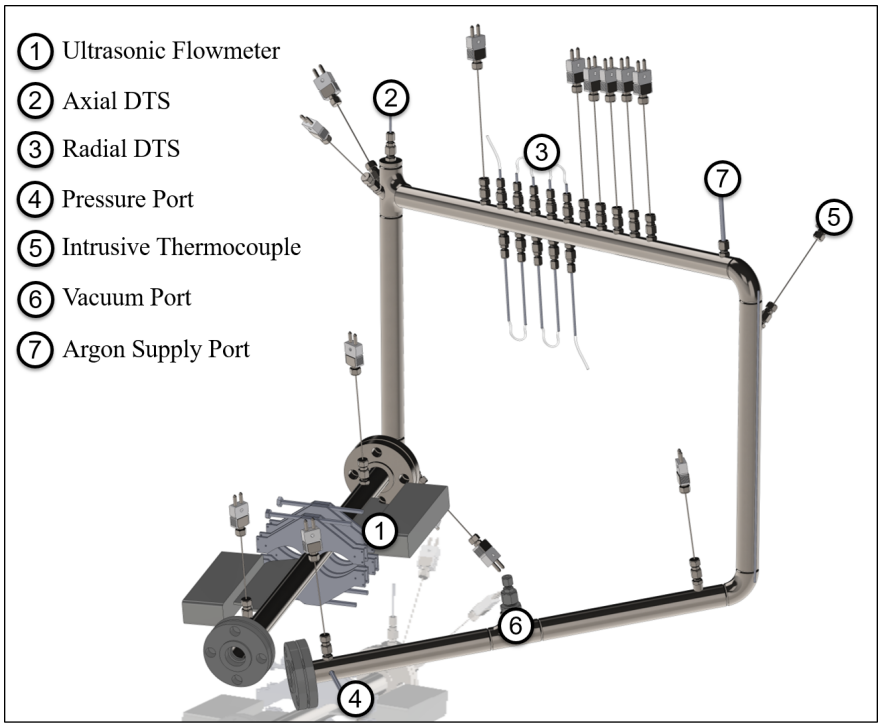

Figure 3.2: Overview of the test loop with installed instrumentation.[15]

pressure transducer. Leg 2 contains a means to make axial DTS measurements with the OFS. Since the fiber can not come into direct contact with the molten salt, a 3.175mm thick walled SS316 tube is passed through and secured via compression fittings at each end of the pipe section, and the fiber is fed through it. At each end of leg 2, there are thermocouples that are used as a source of calibration for the fiber. The same installation method is used on Leg 3, which has 5 fiber sections spaced 38mm apart that allow for radial temperature distributions to be measured. The first and second thermocouples on Leg 3 are used for calibration of this section of OFS. This leg also contains an argon inlet port to maintain an inert environment within the test loop. The 4th leg contains only thermocouple measurements, and leg 5 contains thermocouples, as well as a vacuum port, and a port for the low pressure side of the pressure transducer. Figure 3.3 below shows a detailed view of the physical setup of both the axial and radial OFS for distributed temperature measurements.

Pressure, flow and thermocouple measurements are monitored via a National Instruments PXIe-1092 Chassis, which utilizes NI TB-4353 thermocouple cards, and SCB-68A voltage input cards.

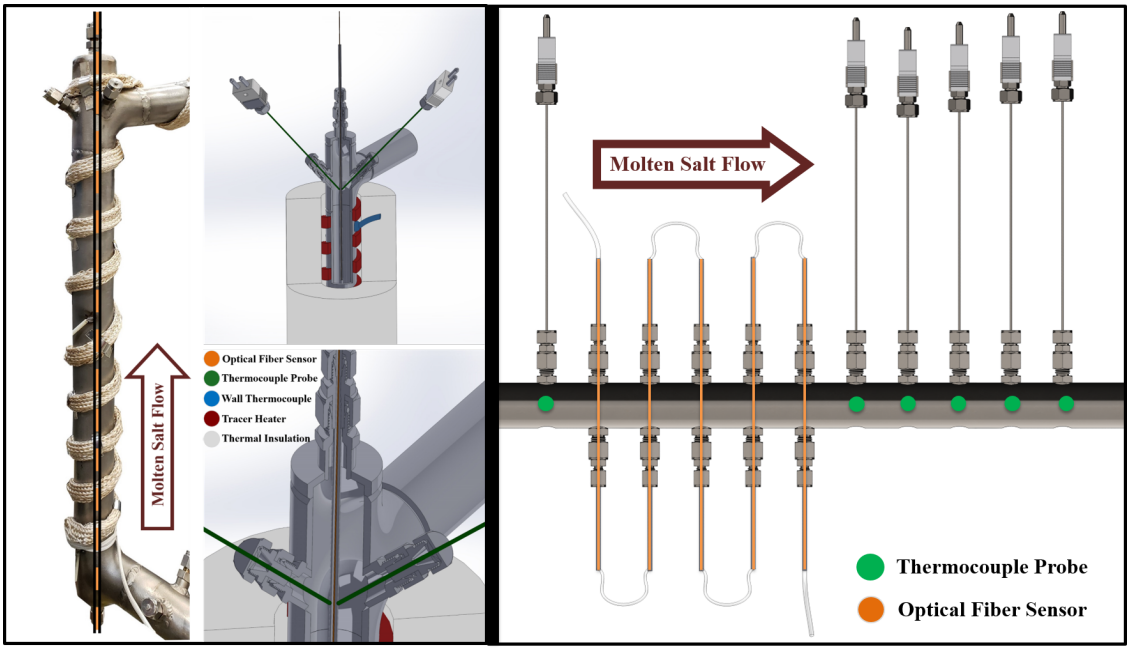

Figure 3.3: Detailed view of the axial (left) and radial (right) OFDTS installation and co-located thermocouple probes.[15]

Data for these instruments is monitored and recorded through a LabVIEW® code. A Programmable Logic Controller (PLC) is also used for control of tracer heater power, pump operation. This allows for safe, hands-off operation of the facility from beginning to end of an experiment. The PLC is also used for visualization of a live view of the measurement values through the use of an Open Platform Communications (OPC) server that relays values between the DAQ and PLC. The OFS interfaces with a LUNA Innovations Inc. Optical Distributed Sensor Interrogator (ODiSI) model 6108 and its data is monitored and recorded with its own software. The details of the instrumentation, including the working principle and construction of Optical Fiber Distributed Temperature Sensors will be discussed in the next chapter, followed by the experimental method used.

4. INSTRUMENTATION OVERVIEW

The instrumentation described briefly in the Facility Overview section will be detailed below. Though results for pressure and flow are not presented in this thesis, they are an important design factor of this facility and the details of these devices will be presented here.

4.1 Differential Pressure Transducer

Pressure drop measurements are important for their ability to validate future system simulations, as well as confirm the output of the flowmeter. A differential pressure measurement system was installed between the inlet and outlet of the test loop to measure the total flow pressure drop. As shown in Fig. 4.1, the system consists of two diaphragms (A) installed at the loop inlet and outlet to interface the molten salt with a sodium-potassium (NaK) filled transfer line(C & C'). These transfer lines connect the diaphragms with a Yokogawa® pressure transmitter (Model: EJA110E)(not shown in figure). This same setup was also used in Arora et al. [15]

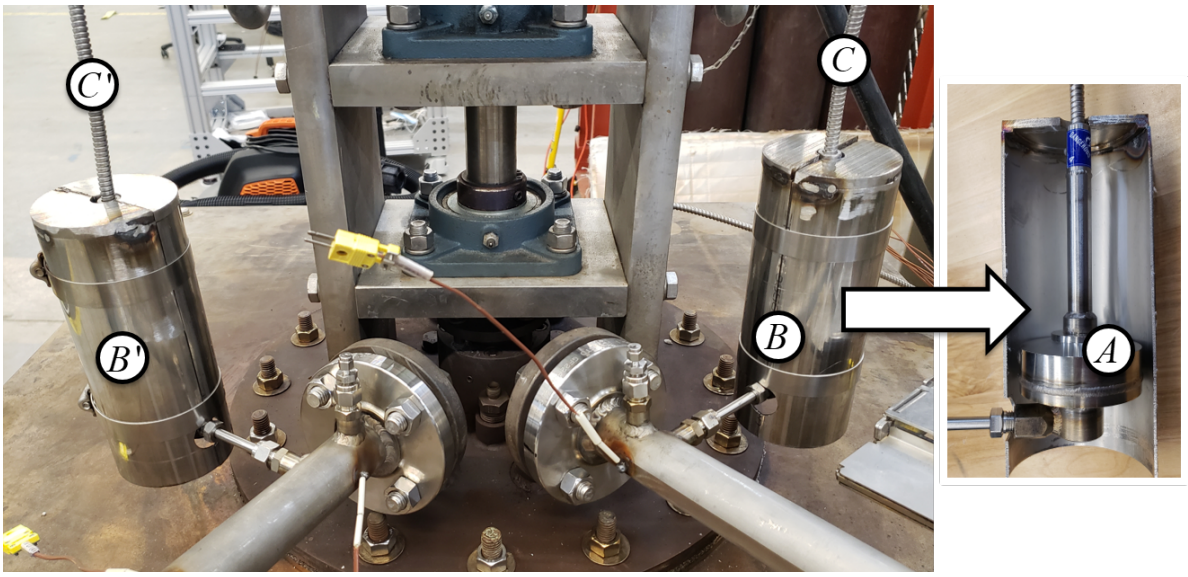

Figure 4.1: Installation of the differential pressure measurement system.[15]

The diaphragms were enclosed in custom fabricated SS316 casings (B & B'), that were wrapped with heating tapes to ensure temperature of the salt-side of the diaphragms is maintained high enough to prevent plugs of FLiNaK from forming. This pressure system interfaced with a data-acquisition (DAQ) system via a Hart Interface Module (HIM), has a measuring span of 4.98 - 498.18 kPa.

4.2 Ultrasonic Flowmeter

As mentioned previously, different methods of flow measurement have been considered for molten salt applications, and non-intrusive methods were conceived to be most desirable. A non-intrusive ultrasonic flowmeter manufactured by FLEXIM® designed for high temperature applications, was selected for flow rate measurements in this work.

The principle of this technology is based on the estimation of the difference in the transit time of an ultrasound that is emitted and received by two wave injectors, in combination with the known speed of sound of the fluid. This technique is considered one of the most viable options for flow measurements in molten salts based on a research by ORNL [16]. Measurements have been conducted by Pantano [17] in low-temperature water flows setups using the same device, but successful use of the flow meter in prototypical molten salt environments has not been confirmed. The measurement's reliability and stability using this technique depends on several installation and configuration parameters including the mounting orientation and distance between the clamp-on transducers, the number of sound paths of the ultrasound wave [18], and the pipe surface conditioning. Prior to generating successful measurements, sensitivity and parametric studies have been conducted in order to identify the optimal selection of these parameters based on the operating conditions of the loop. After various shakedown tests, successful measurements have been recorded in this facility, as presented in Arora et al. [15].

4.3 Thermocouples

Two different methods of thermocouple measurements are utilized in this facility. Sixteen K-type thermocouple probes manufactured by OMEGA Engineering (Model: KQ316SS-116G-12),

are installed at different locations in the facility to measure the salt temperature, as well as act as the reference for control of heating tape power to control temperature of the test loop through the PLC. Probes were installed in the sump tank, legs' inlet and outlet, and at multiple locations along each leg of the test loop. The probe readings are also used as reference temperature measurement to provide calibration for the distributed temperature sensors located on two segments of the test loop. There are also 53 K-type wall thermocouples installed along the walls of the test loop by welding OMEGA K-type extension wire to the pipe. These allow for measurement of the walls' axial and azimuthal temperatures with the purpose of possible future analysis of the convective heat transfer through the pipe.

4.4 OFDTS

With the focus of this thesis being on the results of OFDTS measurements, their measurement principle, construction, and installation method will be discussed in detail below.

4.4.1 Measurement Principle

As mentioned previously, optical fibers provide a means to measure temperature and strain with high spatial resolutions and sensitivity. There are multiple methods and technologies that can be utilized in order to make DTS measurements, as summarized by Ukil et al. [19]. The OFS used in this study works based on the detection of the back-scattering of light from a laser, specifically Rayleigh back-scatter. Back scattered light contains three different spectral components consisting of Rayleigh scattering at the wavelength of the laser source, a Stokes portion at a higher wavelength, and an Anti-Stokes component at a lower wavelength [19]. The Rayleigh Scatter is a random, but stable pattern of reflections that is unique to each fiber as a result of small scale non-homogeneities. This unique reflection signature is stretched under strain which shifts the spectral content [20]. The acquisition of the Rayleigh back-scatter signal and subsequent conversion to a strain or temperature measurement is done via Optical Frequency Domain Reflectometry (OFDR). This technique has been highly regarded for its ability to produce high spatial resolution measurements with a large dynamic range [21]. Kreger et al. [20] also demonstrates the in depth

mathematics behind OFDR, which will be summarized here.

Equation 4.1 describes the optical power P as a function of the tunable laser source source frequency ν.

$$P(\nu) \propto E_R^2 + E_S^2 + 2E_R E_S \cos(2\pi\nu\tau) \tag{4.1}$$

Where E_R and E_S are electric field amplitudes of light transmitted in the reference path of the interferometer and light reflected from the sensor respectively. Here, τ represents the time of flight delay between light in the reference and sensor paths, and is proportional to length difference, L between the interferometer paths and n, the fiber's index of refraction as seen in equation 4.2, where c is the speed of light.

$$\tau = \frac{2nL}{c} \tag{4.2}$$

With this, there is a complex reflection coefficient of the sensor that can be mapped to the delay time τ, by converting the detected fringes collected as a function of frequency, and performing a Fourier transform. The interference fringes will have a frequency, f_{ofdr} that increases corresponding to the reflection event distance from the sensor interrogator.

$$f_{ofdr} = \frac{1}{2\pi}\frac{d}{dt}(2\pi\nu\tau) = \tau\frac{\partial\nu}{\partial t} + \nu\frac{\partial\tau}{\partial t} \tag{4.3}$$

The spatial sampling resolution of the fiber is defined in equation 4.4 below, and is inversely proportional to $\Delta\nu$, the optical frequency scan range.

$$\delta l = \frac{c}{2n}\frac{1}{\Delta\nu} \tag{4.4}$$

When Rayleigh scatter is used, the scatter spectrum is cross correlated in order to determine the spectral shift. According to Kreger et al. [20], it is typically necessary to combine 100 sampled points to form a reasonable spectral shift, which will determine the final measurement spatial

resolution. The tuning rate, $\frac{d\nu}{dt}$, scan range $\Delta\nu$ and sample rate R_s are all linked by the constraint N_{max}, which is the limit on the size of the data array that can be collected.

$$N_{max} = R_s \Delta\nu / (\partial\nu / \partial t) \tag{4.5}$$

The maximum array size from equation 4.5 is important for consideration of the fiber sensors application. Since the scan range influences the strain and temperature range, and the laser tuning rate determines measurement distance, there are ultimately practical trade-offs between measurement spatial and temporal sampling resolutions, as well as power consumption considerations.
All of the aforementioned theory and equations are put into practical use by commercially available sensor interrogators. The hardware used in this study is the Luna Innovations Optical Distributed Sensor Interrogator (ODiSI) model 6108 (figure 4.2 courtesy of Luna Innovations Inc. [22]).

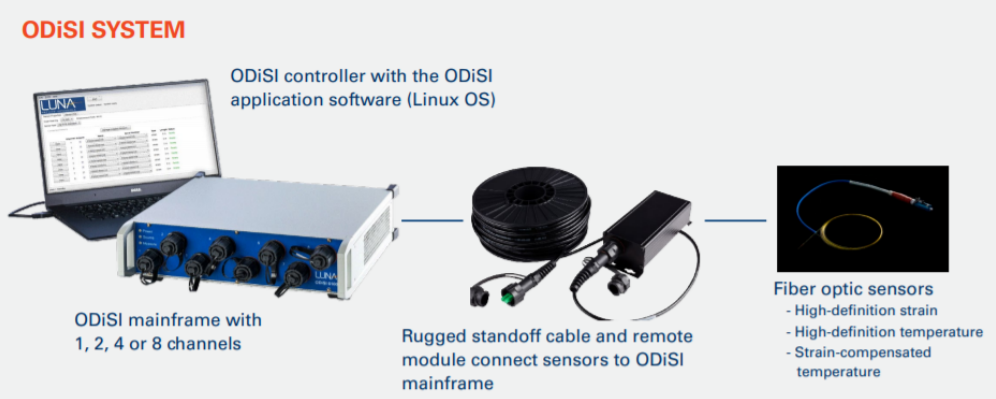

Figure 4.2: Luna ODiSI system overview (Reprint from Luna Innovations Inc, 2020)

This system contains eight channels for monitoring optical fiber sensors, with adjustable spatial resolution capabilities down to 0.65mm. The trade-off between spatial and temporal resolution is adjusted automatically by the software when the spatial resolution is selected. With a a finer spatial resolution comes a courser sampling rate, and this effect is amplified when the number of sensors is increased, which effectively constitutes an overall larger sensor length.

4.4.2 Optical Fiber Sensor Construction

The optical fibers used for distributed temperature or strain measurements have a specific form with a few differences in the construction process depending on the type of fiber being used. Each fiber purchased is a single mode (SM) type optical fiber that utilizes LC type connectors. SM fibers have a smaller core diameter than multi-mode (MM) fibers. This keeps attenuation to a minimum by preventing too many reflections. The bandwidth of SM fibers is also not limited by its light mode like MM fibers. Though more expensive, SM fibers were determined to be a good choice for ensuring success in high resolution temperature measurements.

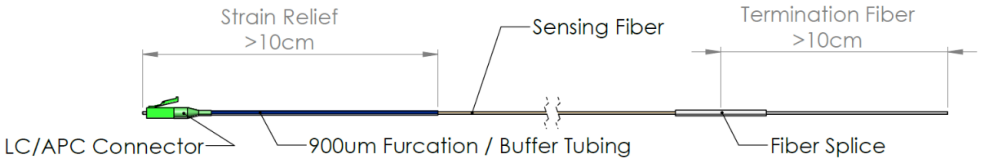

Figure 4.3: Anatomy of constructed fiber sensor (Reprint from Luna Innovations Inc, 2020)

Each fiber sensor is constructed in the same way, with the only difference being the method used to strip the coating from the ends of the fiber, depending on the type being used. The fibers being tested include a polyimide, aluminum, and hybrid gold/carbon coating. While differing in coating, these fibers are also rated to different maximum temperatures (a property of the coating), and have slight variations in optical parameters. These particular fibers were chosen in order to determine the effect of coating, and if these fibers will operate successfully, and with multiple thermal cycles of high temperatures. The overview on fiber types and their properties is shown in the Experimental Methods section following this instrumentation section.

Figure 4.3 shows an example of the typical fiber sensor construction, similar to that which is used in this study, courtesy of Luna Innovations Inc. technical documents. A typical fiber consists of the sensor fiber itself, cut to the necessary length for the application, with each end stripped of its coating. After stripping, the exposed fiber end is cleaved to create a flat end face with a

Precision Rate Optics cleaving tool, and then cleaned with alcohol. One end is then spliced to an LC connector with similar fiber coating diameter. Splicing is done with a Precision Rated Optics OFS-935C arc splicer. The other end of the fiber sensor is spliced to a coreless fiber that acts as the termination of the sensor. The coreless fiber used for all sensors in this study is an OFS Optics F26521 coreless fiber. This termination is important based on the measurement principle described above, in which the termination fiber contains no waveguide (core), allowing it to minimize back reflections at the sensor end point. An image of the devices used in this construction process is shown in figure 4.4 below courtesy of Precision Rated Optics [23].

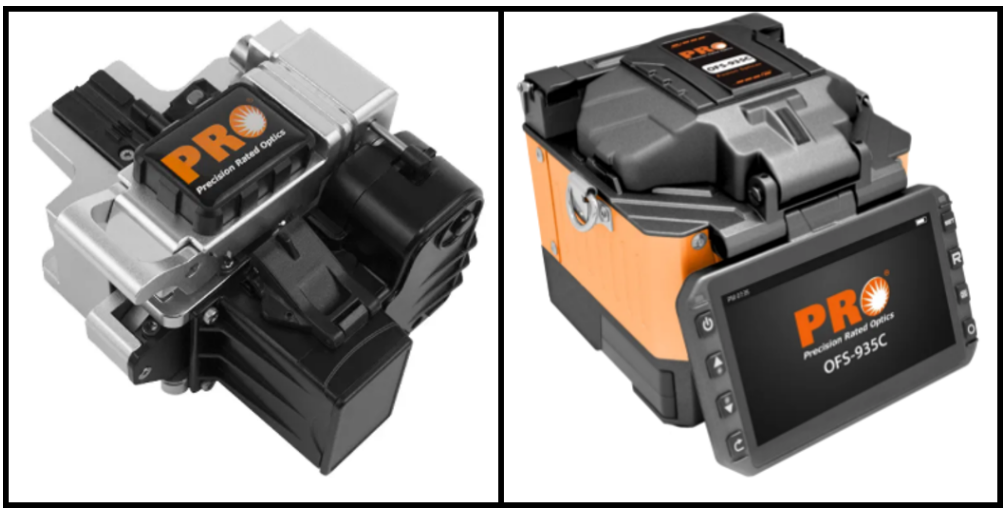

Figure 4.4: Fiber end cleaver (left) and arc splicer (right) (Reprint from Precision Rated Optics, 2020)

As mentioned previously, each fiber used in this study is manufactured with different exterior coatings, requiring different methods of stripping the coating before the splicing operation. The simplest of these is the Polyimide coated fiber, which requires only mechanical stripping. This is done with a Precision Rated Optics JIC-375 three hole fiber optic stripper. The aluminum coated fiber must be chemically etched with a solution of 1 ounce of Sodium Hydroxide (NaOH), dissolved in 30 mL of water. 1 to 1.5 inches of the fiber end is immersed into the solution for 2 minutes. This process is done per recommendation of [24], and is best done with fresh warm so-

lution. The stripped fiber is then cleaned with acetone, and wiped with KimWipe® delicate task wipers. Similar to the aluminum stripping process, the hybrid carbon/gold coated fiber is chemically stripped with a solution of Aqua-Regia. This is a mixture of Hydrochloric Acid (HCl) and Nitric Acid (HNO3) in a 4 to 1 volumetric ratio. Due to the corrosive nature and toxic fumes produced by this solution, the process was performed in a well ventilated glove box, with the acids neutralized and disposed of safely following the process.

4.4.3 OFDTS Installation and Setup

After OFS construction, the sensor is connected to the Luna ODiSI 6108 Remote Module and subsequently fed through the Stainless Steel capillary tubings installed in the test loop. As mentioned in the facility overview section, these tubings are 3.175mm OD, and are thick walled to inhibit bending. These are secured in the loop via compression fittings with the purpose of eliminating vibrations of the tubing that may be induced by the pump or the flow of salt. There is also some room for the fiber to move within the capillary in order to reduce any strain that would be caused during installation.

Fiber sections that remain outside of the capillary tubings are protected through the use of PTFE plastic tubings, and heat shrink is used on those portions that enter and exit the stainless-steel tubings to prevent it from slipping off. Figure 4.5 below shows a constructed fiber installed in the loop.

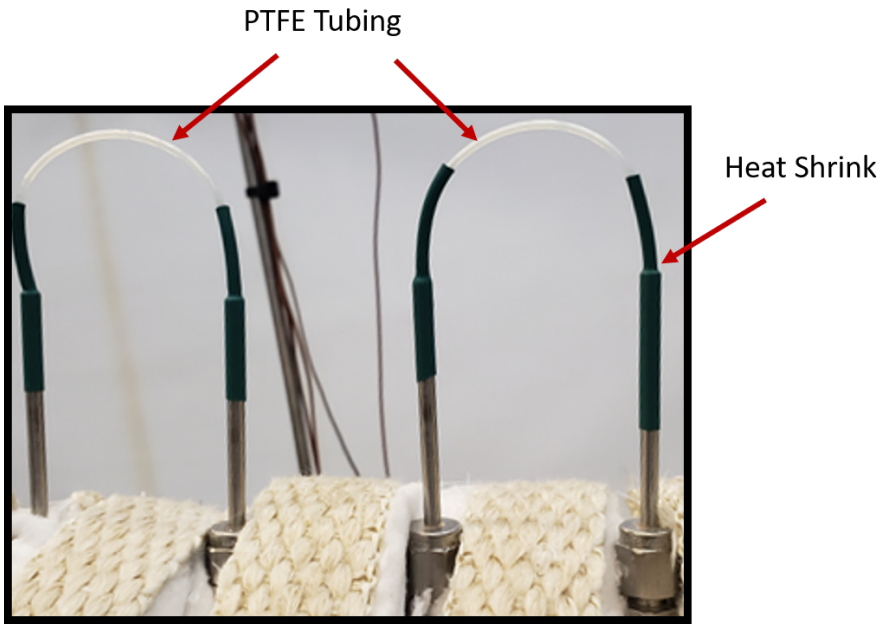

Figure 4.5: OFS installed in Leg 3 of the test loop with protective tubing and heat shrink

With the sensor installed in the desired section of the test loop and connected to the ODiSI remote module, it must then be identified with a unique "sensor key". The ODiSI device constructs a Rayleigh Backscatter profile of the fiber, and saves this unique spectrum in order to identify each specific sensor once it is connected. This keying process is performed at room temperature so that any strain inherent in the installed fiber is recognized and subsequently set to zero before any heating is done. An example of one such backscatter profile is shown in figure 4.6 below indicating the sensor length and the beginning of the termination coreless fiber. The software also indicates the total sensor length as well as the magnitude of signal loss from the connector and termination splices.

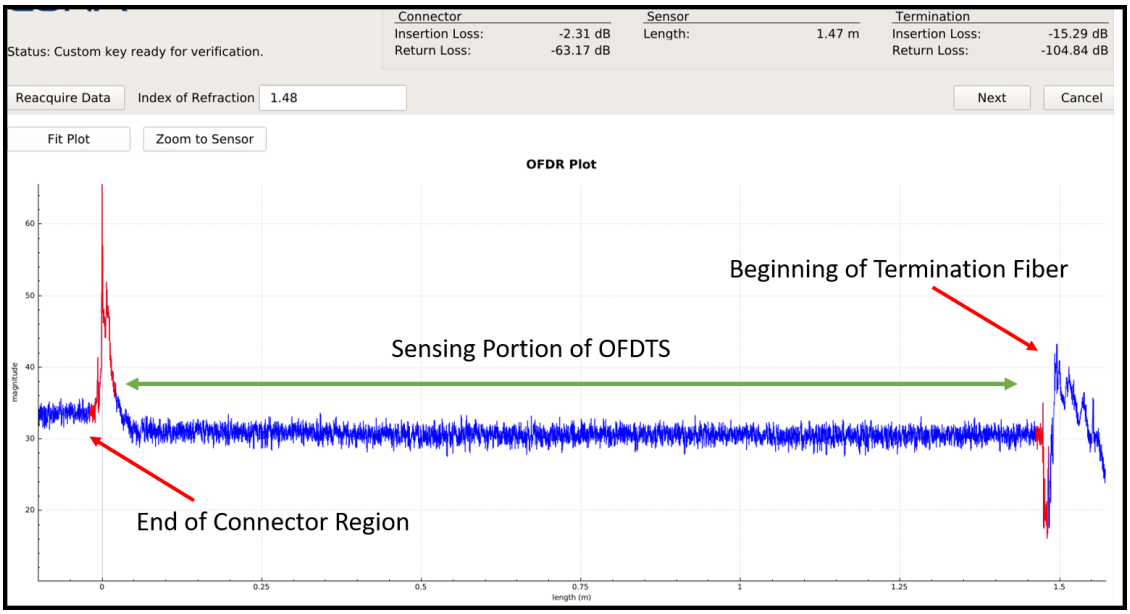

Figure 4.6: OFDR plot showing unique backscatter of installed OFDTS

With each sensor installed in the loop and keyed in the ODiSI software, the OFDTS are ready for data collection following the heating and pumping of salt through the loop. Tests can then be conducted with the goal of determining any differences in fiber coating on the success or response time, as well as any optimum installation or segment lengths. The general experimental method of conducting tests is discussed in the next section.

5. EXPERIMENTAL METHOD & TEST CONDITIONS

Experiments were conducted at an operating temperature of 600°C to guarantee an adequate margin to the FLiNaK solidification temperature (454°C), and preventing the formation of localized plugs. Prior to turning the pump on, the test loop is flushed with argon gas, along with intermittent vacuuming to sustain an inert environment and inhibit chemical attack from the molten salt on metal components [25]. An experiment begins with turning on the sump tank's heaters to melt the 25 kg of FLiNaK in the tank. This is done in 200°C increments with a final temperature of 600°C. Simultaneously, the trace heaters on the test loop are incrementally increased to a final temperature of 550°C. This temperature difference allows for a confirmation of salt flow by monitoring thermocouple response during pumping. It also allows for visualization of the temperature increase by the OFS for analysis. During this heating process, the tank and loop are vacuumed and flushed with Argon. When the experiment begins, the pump will be turned on using the PLC to a speed of 25 Hz to establish flow, which has been confirmed from preliminary shakedown testing. Before this pumping operation, the OFS sensors will read initial values of temperature due to the preheating of the test loop. For each installed fiber these values are set to zero by performing a tare in the LUNA ODiSI provided software. This step ensures no residual strain or thermal stresses are included in the data when pumping begins. An example is shown in figure 5.1 below.

With the goal of collecting successful measurements with optical fibers in this high temperature environment, multiple configurations, as well as types of fibers must be utilized. For example, fibers from different manufacturers with different external coatings are tested. Fibers under consideration are polyimide coated, aluminum coated, as well as a hybrid gold-carbon coated fiber. These fibers are specified by the manufacturers to have maximum operating temperatures below the 600°C operating temperature of the facility. One facet of this experiment is confirming the use of these sensors despite these limitations that are often set based on the coating being used. Table 5.1 below details the manufacturer specifications of the fibers being tested.

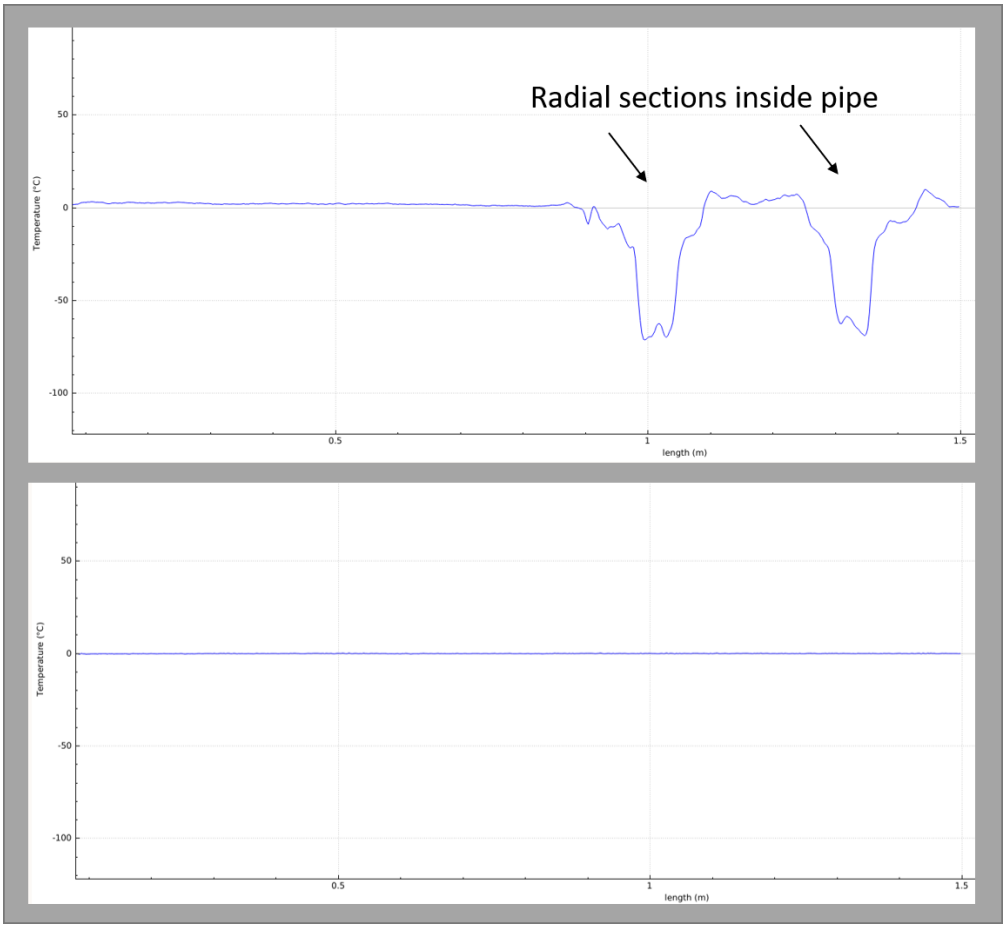

Figure 5.1: An untared (Top) and tared (Bottom) OFS section

Table 5.1: Fiber Specifications

Fiber Name	Coating	Temp Limit
ClearLite®POLY 1310 21 NA	Polyimide (Pyrocoat)	300°C
IX Blue IXF-RAD-SM-1550-014-AL	Aluminum	400°C
AFL Verillon VHT500 Ultra	Hybrid Gold-Carbon	500°C

Due to the design of the OFS configuration of this facility, a single fiber can be fed through the entire axial and 5 radial segments, or multiple different fibers can be monitored at the same time on different segments. Thus, Table 5.2 below shows an outline of configurations that have been performed in this study.

Images detailing each configuration can be found in Appendix A.

Table 5.2: Experimental OFS Configurations

	Axial Segment	Radial Segments
Configuration 1	Polyimide Coated	Polyimide Coated
Configuration 2	Aluminum Coated	Aluminum Coated
Configuration 3	Hybrid Gold-Carbon	Combination of Aluminum, Polyimide, Hybrid

Due to this high temperature environment, long segments may be more effected by thermal strain, and therefore be more prone to breaking. Therefore, shorter segments of the same type of fiber are being investigated rather than only testing these fibers in long segments across the axial and radial sections.

The calibration techniques applied before processing the data is discussed in the next section, along with the uncertainty of the measurement devices.

6. CALIBRATION & UNCERTAINTY ANALYSIS

6.1 Calibration

In order to maintain accuracy of thermocouple readings for subsequent OFS calibration, the thermocouples are calibrated using a sensitive Resistance Temperature Detector (RTD) as a reference source. The device used is a Fluke® 5624 RTD probe connected to a Fluke® 1524 thermometer readout. A three point calibration is performed at ambient temperature, 480°C and 700°C. For the ambient data point, the thermocouple and RTD probe are left inside a wrap of ceramic fiber insulation for ten minutes to ensure they are both reading a steady temperature inside the insulation. Then, data is recorded for both probes for six minutes. For the last two calibration points, a furnace with an open insertion point at the top is used. The furnace is set to the desired temperature with the probes inserted, and after the furnace reaches this temperature, the probes' readings are recorded for six minutes. To create a calibration curve for the thermocouples, the recorded data at the three temperatures for each probe is time averaged over the six minute recording interval. An image of an example of the resulting calibration curve is seen in Figure 6.1.

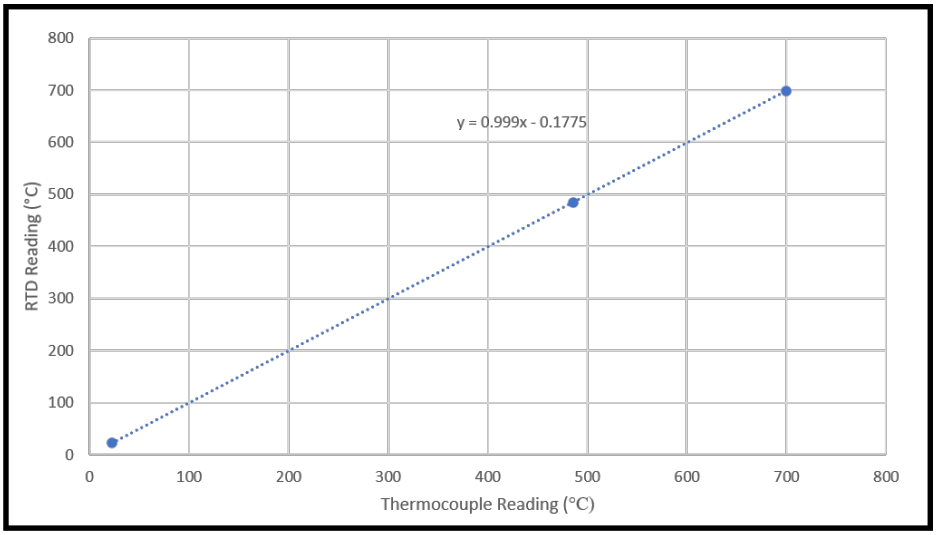

Figure 6.1: Resulting thermocouple calibration curve from RTD

Following collection of the OFDTS transient response of the molten salt flow, the data must be calibrated to reflect the real temperature values, rather than the relative values collected by the ODiSI system. As mentioned in the facility description section, there are thermocouples located at the top and bottom of the axial fiber section, as well as before and after the radial fiber section. These are used as the reference measurements from which a calibration curve is created for each individual portion of fiber within the pipe.

First, a plot of the thermocouple temperature vs time is generated in MATLAB® showing the increase in temperature before and after pumping begins. A time average of the before pumping temperature, and the steady state temperature of the salt flow is found. An identical plot is made with the fiber section of interest, showing the un-calibrated temperature vs time. Because the thermocouple tips measure temperature at the center of the pipe, the center point of the fiber is used for this plot when calibrating radial segments, and points adjacent to the thermocouple are used for the axial segment. Again, a time average of the before and after pumping temperatures are calculated. With these four values, a calibration equation can be generated and applied to that entire portion of fiber which converts the relative measurement values to calibrated temperature values. This process is done for the first and last radial segments of fiber as well as the axial segment. For the three radial segments in between the first and last, there is no reference thermocouples. Therefore, the values for generating the calibration equations are found by a linear interpolation between the existing reference thermocouples using the average before and after pumping temperature that was collected for each. A qualitative visualization of this interpolation on the radial fiber section is shown in Figure 6.2 below.

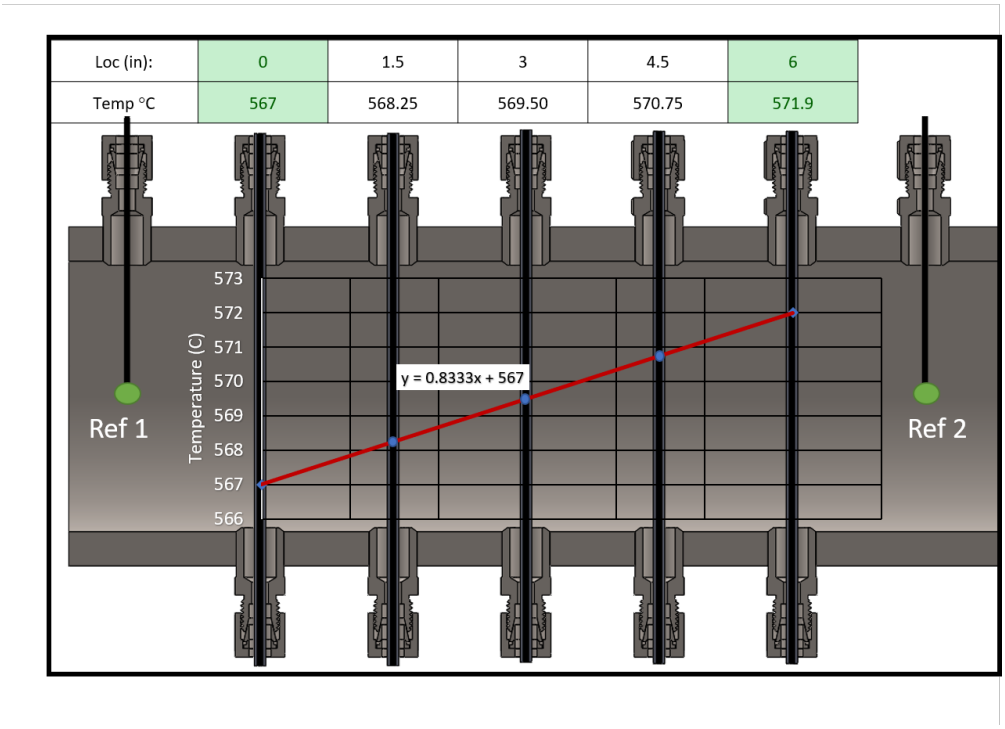

Figure 6.2: Interpolation of reference temperatures for a specific fiber calibration

A similar interpolation is done to estimate the salt steady flow temperature at these intermediate segments. This results in a two point linear calibration curve for each radial segment. It should be noted that this calibration process is performed for each data set that is produced from an experiment, as the reference temperatures will be unique each time the facility is utilized. Figure 6.3 below shows an example of a set of calibration curves that were generated for one set of radial fiber data used in this thesis. The calibration values used are those seen in the example from figure 6.2 above.

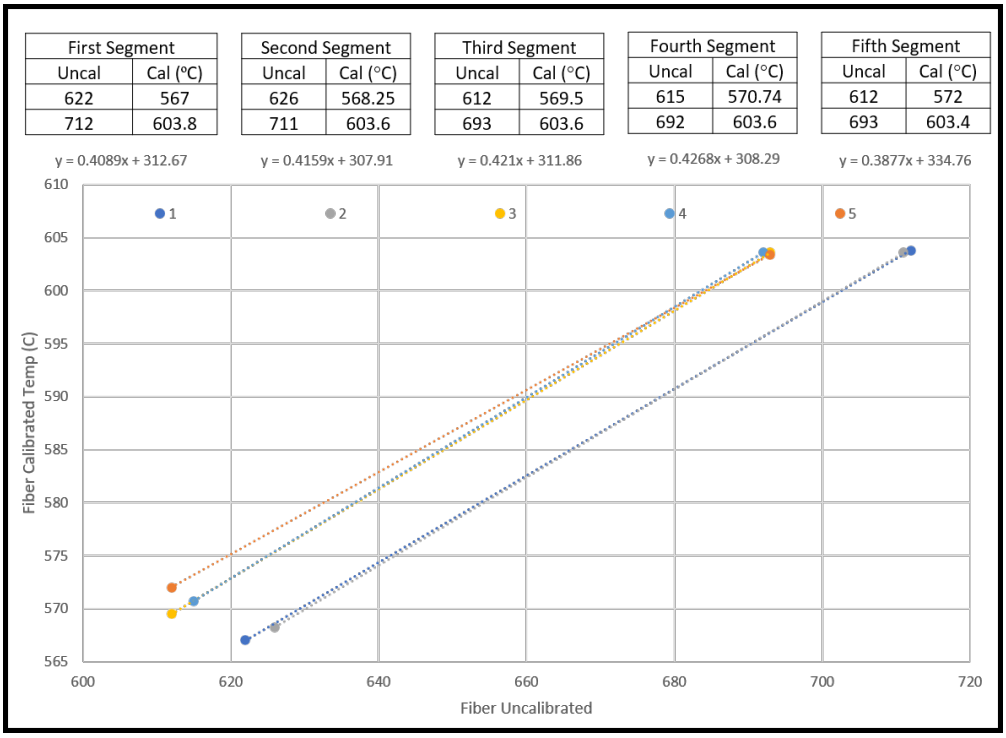

Figure 6.3: Radial OFDTS calibration equations for one data set

There is also some uncertainty in both temperature measurement devices that must be considered. The uncertainty sources of the thermocouple and OFDTS are discussed in detail in the next sections below.

6.2 Thermocouple Uncertainty

The uncertainty of the K-Type thermocouple probes is estimated by considering three main sources of error. These are the calibration standard deviation (σ_{cal}), the manufacturer specified error of the K-type thermocouple and the error in the reference device used for the calibration (σ_{RTD}). Eq. 6.1 below is used to estimate the total uncertainty of the K-type thermocouple probes.

$$\sigma_{TC}^2 = \sigma_{cal}^2 + +\sigma_{device}^2 + \sigma_{RTD}^2 \tag{6.1}$$

The calibration uncertainty comes from the standard deviation of the difference between ob-

served (thermocouple measurements) and predicted (calibration curve) values [26], and was found to be 0.33°C. The combined accuracy of the reference thermometer and RTD probe (σ_{RTD}) is reported to be 0.031°C, and the error of the K-type thermocouple specified by the manufacturer (σ_{device}) is 1.1°C. Therefore using Eq. 6.1, the total uncertainty (2σ) is $\pm$ 2.30°C.

6.3 OFDTS Uncertainty

To estimate the uncertainty of OFDTS measurements, a similar approach as done by Holler et al. [27] was used, which was based on the same method used by Lomperski et al. [28]. Equation 6.2 below shows the contributing factors considered in this analysis.

$$\sigma^2_{OFDTS} = \sigma^2_{K_T} + \sigma^2_{\epsilon} + \sigma^2_{ref} + \sigma^2_{ODiSI} + \sigma^2_{RH} \tag{6.2}$$

Here, σ_{K_T} is uncertainty estimated due to material properties of the silica fiber[28], σ_{ϵ} is uncertainty due to any strain on the OFDTS, σ_{ref} is error in co-located K-type thermocouple probes used as a reference and σ_{ODiSI} refers to the manufacturer provided uncertainty for the LUNA ODiSI 6108.

The term σ_{K_T}, is taken from Lomperski et al. [28] and is $\pm$ 1°C. Since a stainless-steel tubing is used, there is no strain on the fiber hence σ_{ϵ} is negligible. The σ_{RH} term refers to the error due to relative humidity, and applies to the polyimide fiber due to the coatings hygroscopic nature. The operating temperatures reached in this study are sufficiently high to vaporize the polyimide coating of the OFDTS, while maintaining reliable response of the silica fiber core. Hence this term σ_{RH} is negligible. The term σ_{ODiSI} is reported by the ODiSI 6108 data sheet to be $\pm$ 1.6°C for the spatial resolution selected in this study. With all sources of error considered, the total propagated uncertainty in the OFDTS (2σ) is $\pm$ 4.41°C.

7. RESULTS AND DISCUSSION

Experimental results were obtained for OFDTS in tests where a single segment of Polyimide coated fiber was run through the axial and the five radial segments, as well as tests with an axial gold coated fiber, and a combination of OFDTS types in the radial segments. Tests run with a single segment of Aluminum coated fiber through the test section were not successful due to failure during heating. These results are summarized below as follows with temperature profiles, normalized temperature responses and a summary of high temperature exposure time of the OFDTS.

7.1 Qualitative and Quantitative OFDTS Response

Here, the Polyimide results are shown, followed by the tests in which multiple fiber coatings were used. Then a 2-D temperature field was constructed to visualize salt front development.

7.1.1 Polyimide Single OFDTS (Configuration 1)

These results capture the OFDTS transient response from a pump speed set to 25 Hz, corresponding to 70 lpm. First the axial temperature profile of leg 2 is generated, and seen in figure 7.1a below. The data for this configuration was captured with a 0.65 mm spatial resolution.

It can be seen that at Time(t) = 0, the axial temperature distribution has a cosine profile. This is due to uneven heating and a constant heat flux from the tracer heaters. There is no salt flowing through the test loop at this time instance. As we progress through time, a change in the temperature profile is seen to occur corresponding to the direction of flow of molten salt.

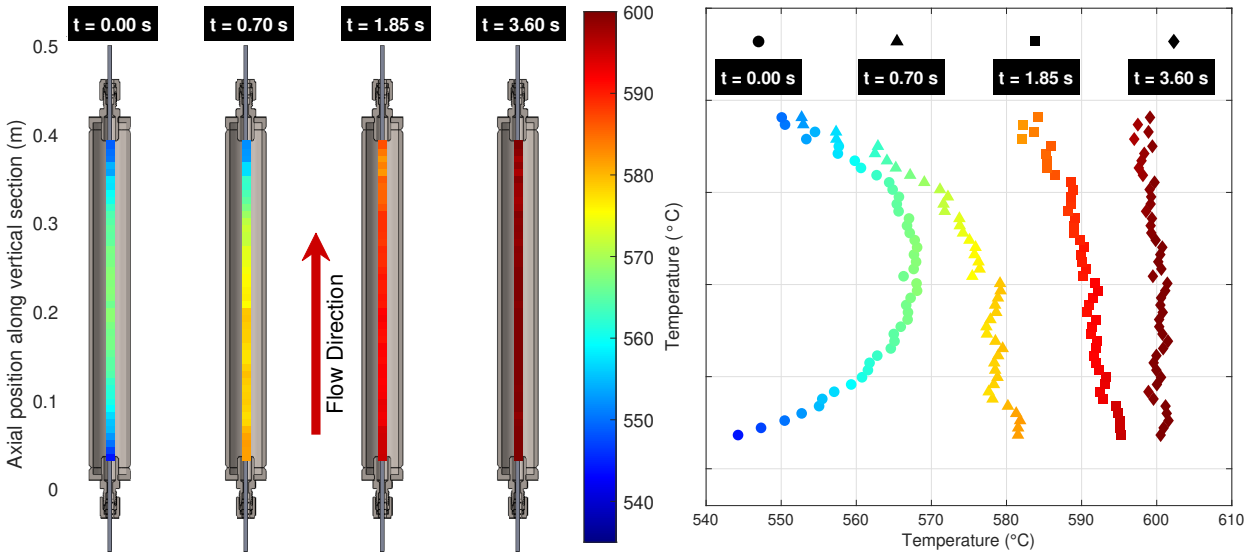

Figure 7.1: Time evolution of the axial OFDTS temperature profiles. Color contour (a); Temperature profiles (b)[15]

The radial OFDTS response for this same configuration was also recorded. Figure 7.2 shows this distribution of temperature profiles of the five radial OFDTS segments as a time evolution. Time(t) = 0 sec again represents the temperature of the pre-heated loop before the salt flow is established. Progressing in time, it is seen that the temperature of first radial segment (Fiber Segment 1) rapidly increases since it is the first to register the temperature of the hot salt. Time(t)= 3.95 sec shows the other segments following in the order that they are located along the horizontal section. It is also evident from these time instances that the increase in temperature begins at the bottom of the pipe section, depicting the molten salt filling up this section. At Time(t) = 4.62 sec, flow is fully established within the test loop and the time-averaged temperature profiles are shown in the bottom right sub-figure. This is done to account for fluctuations in the OFDTS response due to vibrations induced on the tube containing the OFDTS.

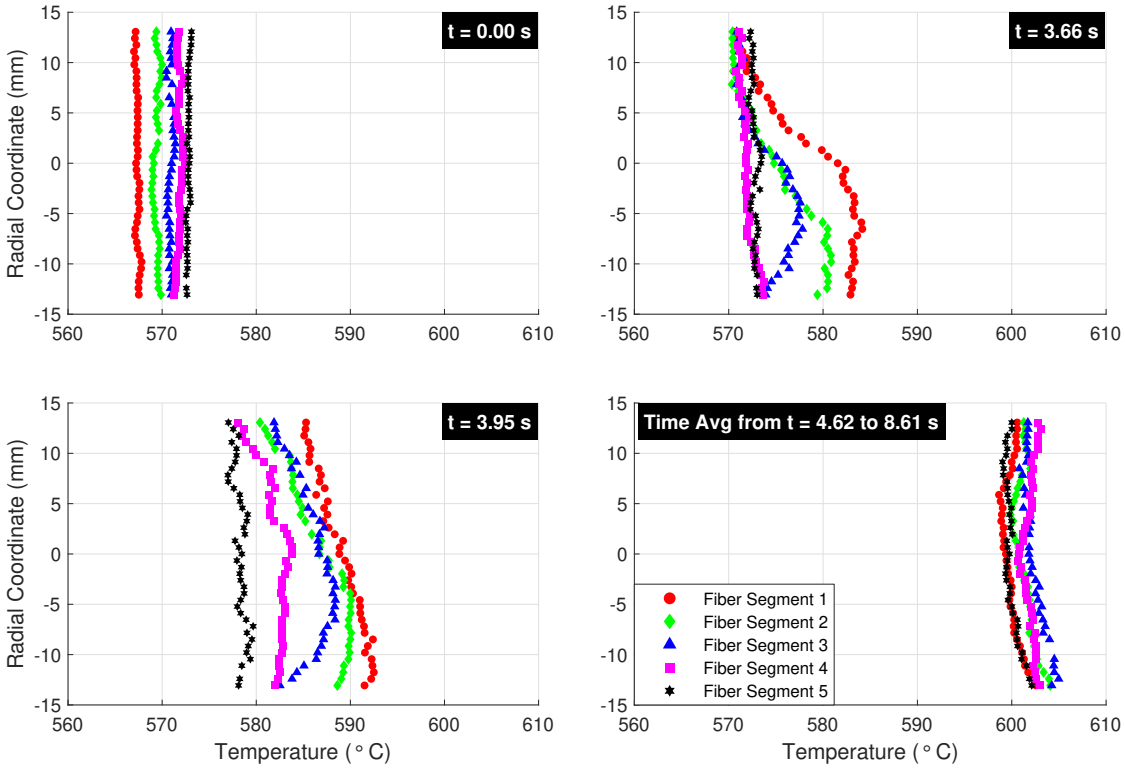

Figure 7.2: Time evolution of the radial OFDTS temperature profiles.[15]

This data is also represented as a qualitative color map in figure 7.3. As a note, each OFDTS segment is 38 mm apart.

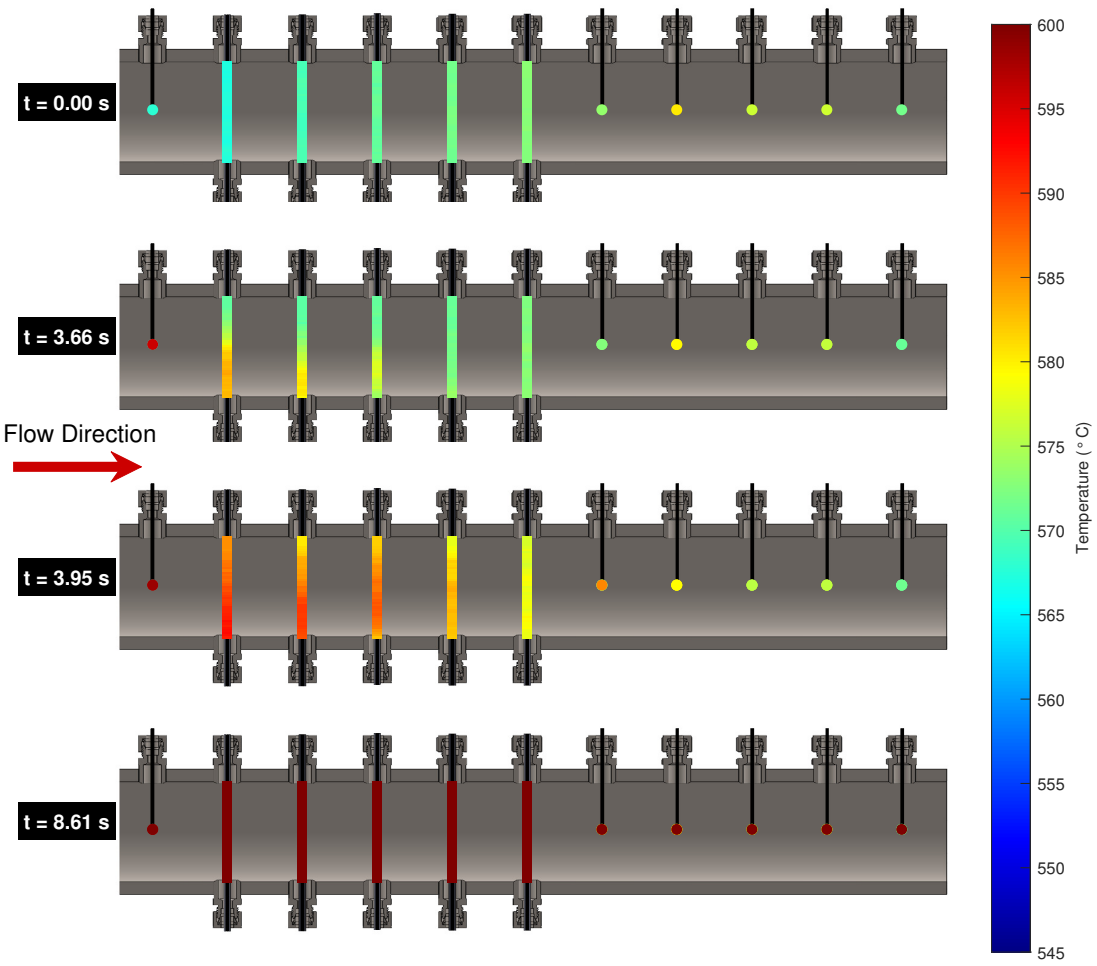

Figure 7.3: Time evolution of the temperature profile from the radial OFDTS and thermocouple measurements. (Geometry not to scale)[15]

7.1.2 2-D Temperature Field Reconstruction

The results from this configuration were also used to develop a two-dimensional temperature field to visualize the molten salt front development. With a spatial resolution of 0.65 mm, there lies 41 OFDTS measurement points within the diameter of the pipe. In order to reduce noise fluctuations, this data at each point on each segment was first averaged with its two leading and two lagging time instances.This original set of OFDTS data can be regarded as a course mesh with a 41x5 grid (41 points along 5 fiber segments). This is refined through a two-dimensional bi-linear interpolation. The refined mesh (41x234) maintains the radial spacial resolution of points from the

OFDTS measurement, and increases the axial resolution through the addition of the interpolated values. The resulting two-dimensional temperature fields under transient flow conditions are shown in Figure 7.4.

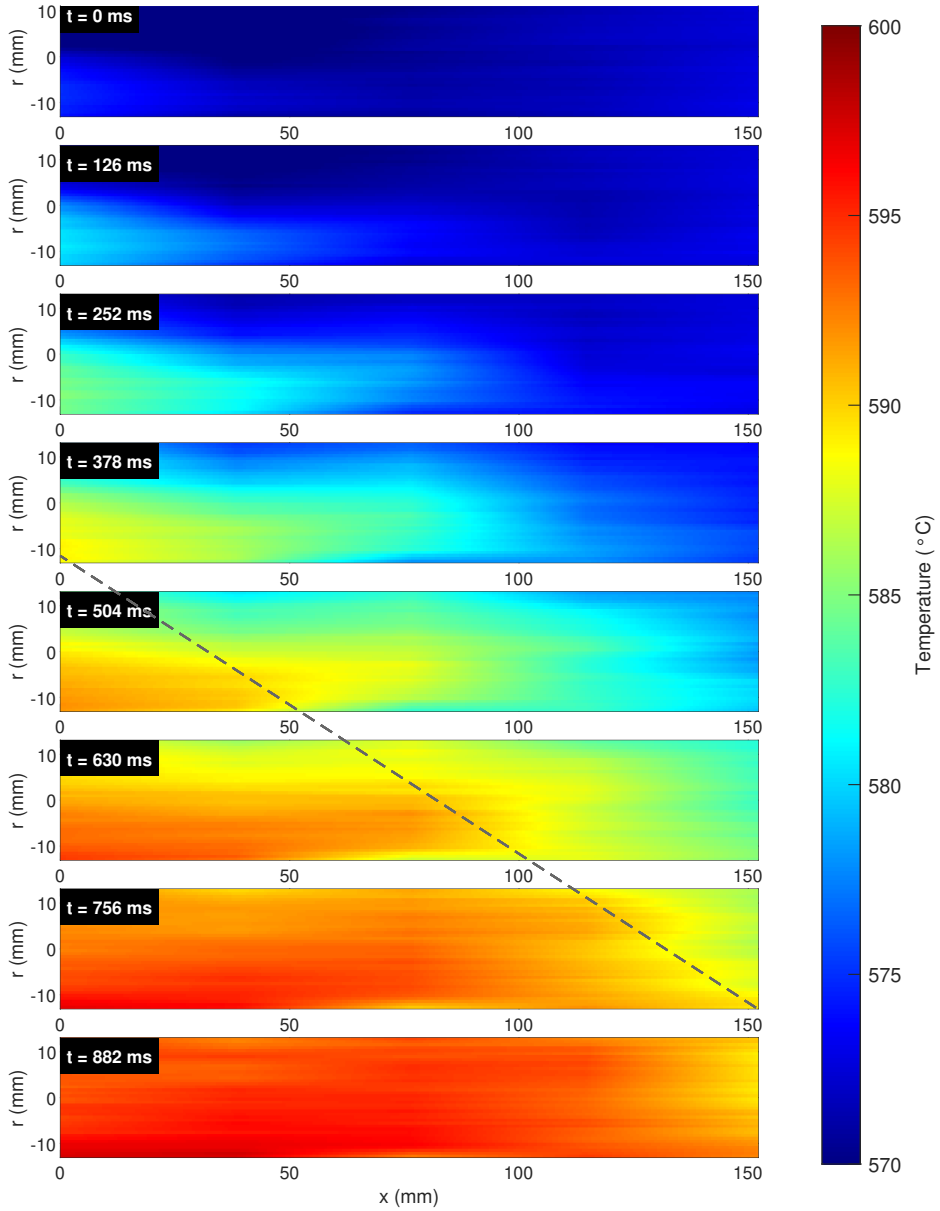

Figure 7.4: Reconstructed two-dimensional temperature field and front development. Snapshots are taken at equal time intervals of 126 ms. The salt front position is interpolated using the dotted line.[15]

This figure can be used to estimate the salt front velocity by determining the time the front takes to span the 150 mm distance between the first and last fiber segment. The dotted line represents the location of the salt front. The average salt front transition velocity was estimated to be 0.39 m/s.

7.1.3 Different OFDTS Combination (Configuration 3)

Though the first configuration (all polyimide) showed success in multiple tests, there was frequent failure that occurred after the cool down of each test. The second configuration (all aluminum) showed no successful result, as the fiber failed during the heating process. This leads to the result of the third configuration in which gold-carbon is used as the axial section and one radial segment, followed by an empty fiber tubing, along with aluminum in two radial segments, and polyimide in the last radial segment. The axial temperature profile for the gold-carbon coated OFDTS is shown in the figure 7.5. Due to trade-offs in spatial resolution and sampling rate when multiple fibers are tested, a spatial resolution of 1.3 mm was used for configuration 3 data.

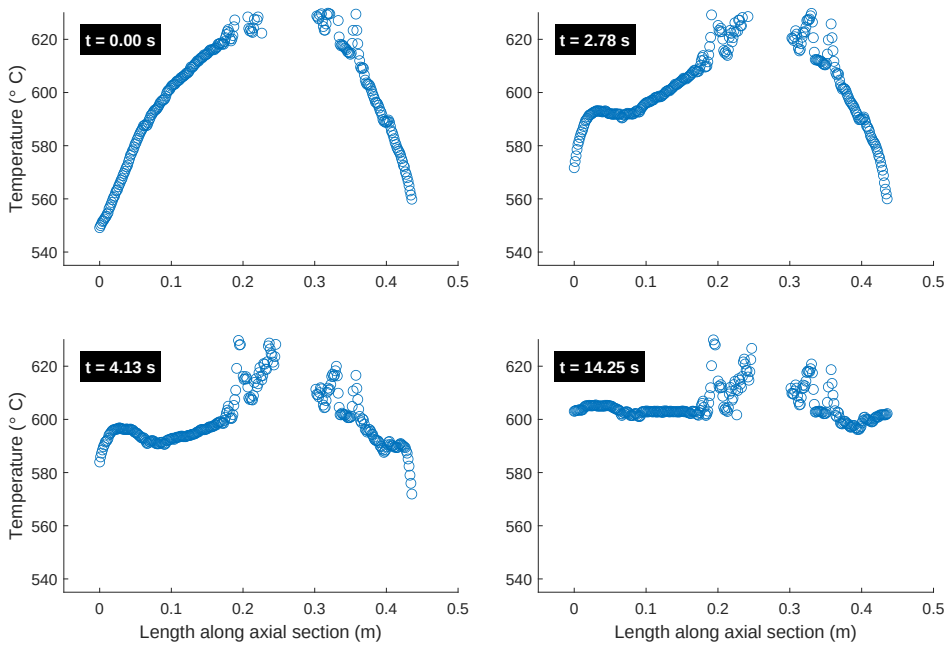

Figure 7.5: Axial temperature profile of gold-carbon coated OFDTS (From test 1)

This figure shows the time evolution of the axial temperature profile. Somewhat differently to

the axial profile of configuration 1 (polyimide), this test section was at a higher temperature during the heating process of the test loop. This resulted in signal loss of the fiber in the middle section, where the temperature was highest. The end points of this profile show some lag in response compared to the rest, indicating that this is a section of fiber just outside of the test section, that is responding to conduction through the capillary tubing.

The radial temperature profiles on leg 3 for this configuration are also shown below.

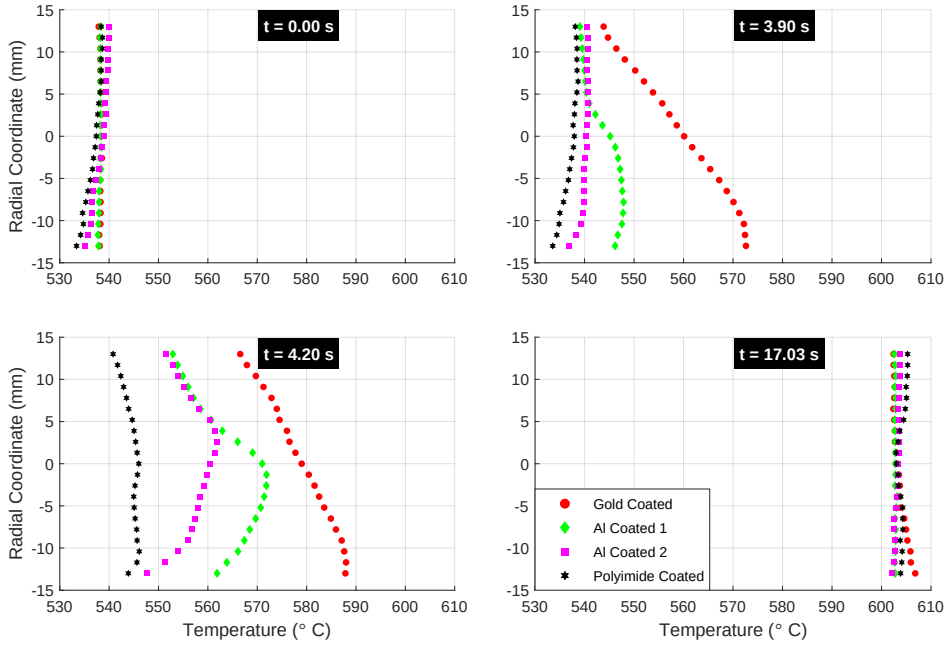

Figure 7.6: Radial temperature profile of different coated OFDTS (From test 1)

Figure 7.6 shows a similar response as that of the polyimide OFDTS in configuration 1. The main difference in response compared to configuration 1 is what seems like a larger gap in response time between the first and second segment. This is because configuration 3 has 4 OFDTS segments, in which there is no measurement between the gold-carbon, and the first aluminum segment, as opposed to the 5 OFDTS in configuration 1.

7.2 Normalized Temperature Response

The temperature responses of the OFDTS for the three tests conducted using Configuration 3 were normalized with their before pumping value to be zero, and steady state salt temperature equal to one. These normalized temperatures are compared in order to show the difference in response times of each OFDTS without regard to their location in the test loop.

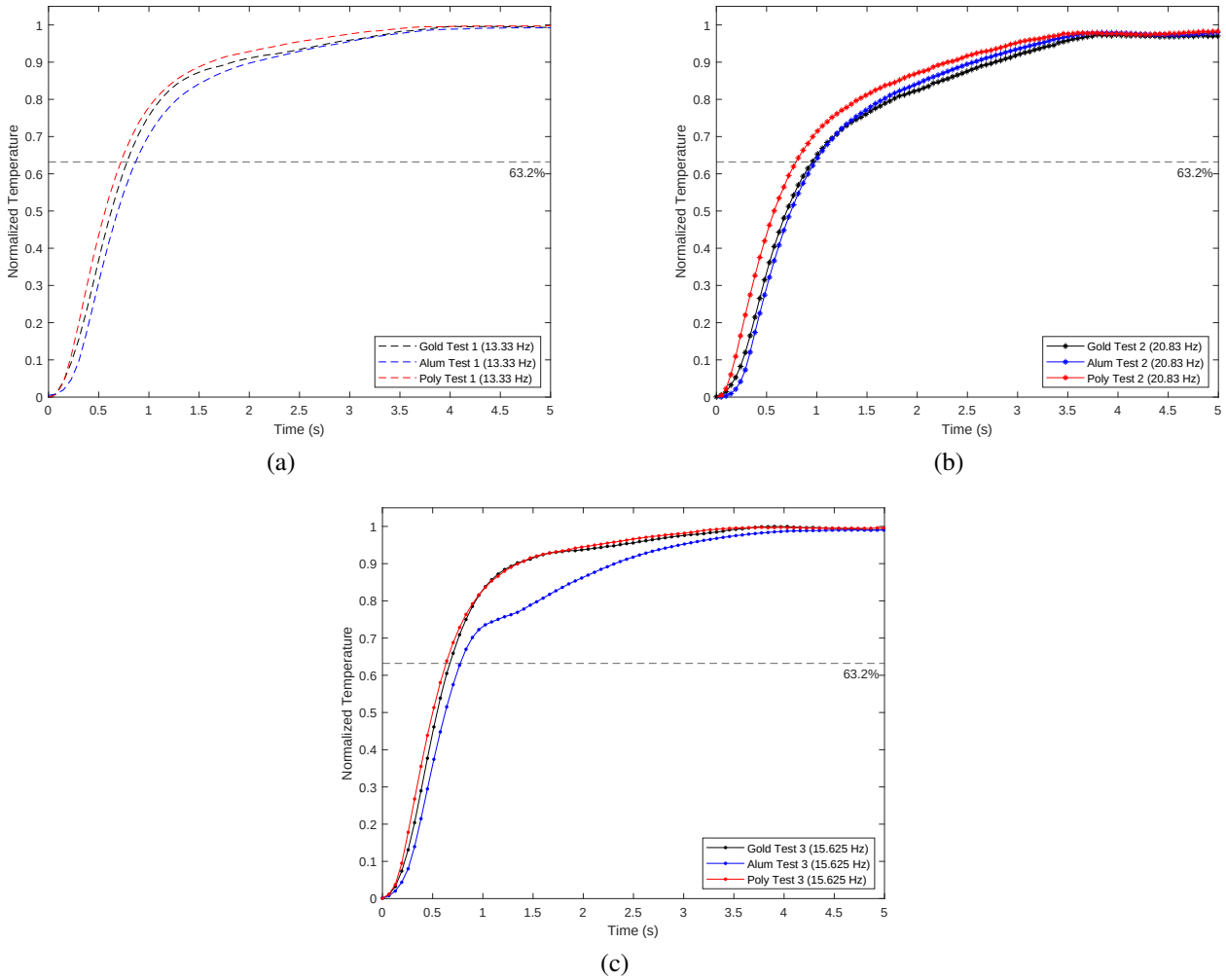

Figure 7.7: Normalized temperature response of configuration 3, Test 1 (a); Test 2 (b), and Test 3 (c)

The time constant, τ of a signals response from 0 to 63.2% of its steady state value is an impor-

tant parameter when analyzing the response of multiple signals. Here, an average value found for each fiber under these three tests was τ = 0.64 sec. This response indicates very little difference between the fiber coatings effect on response time, even under different tests. A likely contributor to the effect of the response time is the installation method, using thick walled capillary tubing, which may have slight differences due to dimensional tolerancing.

The normalized response from configuration 1 testing was also analyzed, and the OFDTS normalization was compared to a normalized thermocouple response.

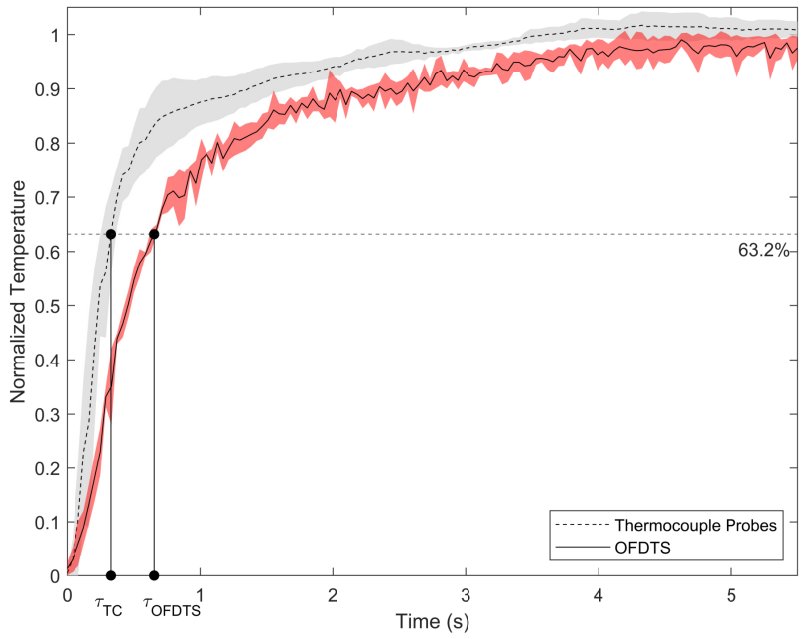

Figure 7.8: Time response of thermocouples and OFDTS. Grey and red shading represents the standard deviation of the thermocouple probes and OFDTS respectively.[15]

The time constant of these normalized responses in figure 7.8 show that the thermocouples responds to temperature variations faster than OFDTS. Here τ_{TC} was found to be 0.332 sec. and the time constant of the OFDTS τ_{OFDTS} is found to be 0.655 sec. This value of OFDTS time constant is in good agreement with the value from configuration 3 tests, performed months later with different fibers.

7.3 Thermal Cycling Summarization

In order to evaluate the possible failure modes of OFDTS in these environments, a summarized table was created to quantify the length of time that each tested OFDTS was exposed to temperatures above 500°C (Preheating loop, and salt pumping), since this is the highest of the temperature ratings of fibers tested. The summary in figure 7.9 below shows each fibers coating, installation, length in test section, time above 500°C, and configuration.

Fiber Type	Installation	Length in test section	Recorded Test Time (Above 500°C)	Config - Test #	
Polyimide	1 Radial	26.64 mm	1.22 hr	Config 3: 1,2,3	→ Survived 3 cycles
Polyimide	Axial + 5 Radial	569.2 mm	4 hr	Config 1: 1,2	→ Failure after each test
Aluminum	2 Radial	53.28 mm	1.04 hr	Config 3: 2,3	→ Survived 2 cycles
Aluminum	Axial + 5 Radial	569.2 mm	1 hr	Config 2: 1	→ Failure during heating
Gold	1 Radial	26.64 mm	1.04 hr	Config 3: 2,3	→ Survived 2 cycles
Gold	Axial	436 mm	0.23 hr	Config 3: 3	→ Failure during heating
Gold	Axial + 1 Radial	462 mm	0.2 hr	Config 3: 1	→ Failure after 1 test

Figure 7.9: Summarization of thermal cycling during different tests

From this data, as well as knowing the result of each test, some conclusions can be drawn based on the ideal installation type/length of OFDTS segments. It was seen that fibers in the axial configuration failed, either after one test, or during the heating process. Here, "failure" means an interruption in the fiber signal in which no data points exist (see Figure 7.5), in addition to an actual broken fiber. These failed segments were not exclusively exposed to high temperatures for a longer time than the shorter (radial) segments, giving evidence that the segment length is the driving factor.

8. SUMMARY

Following the results presented above, some conclusions can be made regarding the success of OFDTS measurements in high temperature environments. Recommendations for the use of OFDTS in future systems will also be made based on these results, as well as the potential for further studies is discussed.

8.1 Conclusions and Recommendations

OFDTS measurements were successfully performed in high temperature molten salt environments under forced convection. Fibers with different coatings, as well as installation configurations were tested. Each type of OFDTS showed success in these environments, proving their effectiveness and potential for use in various different applications (MSRS, CSP etc). Though success was seen by these OFDTS, failure did occur on segments that were installed through the axial segment (>0.4 m in length exposed to high temperature). These failures resulted in a large amount of lost signal in the OFDTS over a portion of its length, or total failure to measure. These failures occurred usually during heating or cooling portions of the test procedure, indicating that some thermal strain on long segments may have negative effects. This is compared to shorter segments installed in the radial (leg 3) portion, which survived multiple tests under similar amounts of operating time as the longer segments. This is also supported by the success of longer OFDTS segments in low temperature environments, as done by Holler et al. [27] with lengths greater than 1 meter. In addition to this conclusion, the time response of the different coated OFDTS was not shown to vary significantly, even compared with the time response of OFDTS in tests conducted months prior. Due to this similarity in response time, the most likely factor is the SS316 capillary tubing that each fiber is installed. Slight variations in response time may be due to variations in the dimensional accuracy of this tubing.

Based on these conclusions, it is recommended to use polyimide fibers, even when operating at these temperatures. These fibers are less expensive than the others tested, and are easier to fabri-

cate due to their stripping method. In addition to this, shorter segments (< 0.4 m) should be utilized when operating at high temperatures, due to the failure seen in segments with this length that were exposed to these temperatures.

8.2 Further Study

Further research on this topic would assist to strengthen the conclusions made in this thesis. More data sets of OFDTS measurements in this facility could provide a means to conduct an in depth repeatability study, and determine a concise total number of thermal cycles before an OFDTS reaches failure. Also, since vibration from the pump is a factor that may facilitate an OFDTS failure mode, a controlled study on OFDTS performance under vibration may be useful for future research.

REFERENCES

[1] Ajay K Misra and J Daniel Whittenberger. Fluoride salts and container materials for thermal energy storage applications in the temperature range 973–1400 k. In *22nd Intersociety Energy Conversion Engineering Conference*, page 9226. American Institute of Aeronautics and Astronautics, 1987.

[2] Jan Uhlíř. Chemistry and technology of molten salt reactors–history and perspectives. *Journal of nuclear materials*, 360(1):6–11, 2007.

[3] Bogdán Yamaji, Attila Aszódi, Máté Kovács, and Gyula Csom. Thermal–hydraulic analyses and experimental modelling of msfr. *Annals of Nuclear Energy*, 64:457–471, 2014.

[4] Piyush Sabharwall, Matt Ebner, Manohar Sohal, Phil Sharpe, et al. Molten salts for high temperature reactors: University of wisconsin molten salt corrosion and flow loop experiments–issues identified and path forward. Technical report, Idaho National Laboratory (INL), 2010.

[5] Rinah Kim, Chan Hee Park, Wook Jae Yoo, and Joo Hyun Moon. Development and characterization of a fiber-optic monitoring system for the key environment variables of the spent nuclear fuel pool at a nuclear power plant. *Annals of Nuclear Energy*, 99:183–192, 2017.

[6] Alex K Sang, Mark E Froggatt, Dawn K Gifford, Stephen T Kreger, and Bryan D Dickerson. One centimeter spatial resolution temperature measurements in a nuclear reactor using rayleigh scatter in optical fiber. *IEEE Sensors Journal*, 8(7):1375–1380, 2008.

[7] James Schneider and Mark Anderson. Using optical fibers to examine thermal mixing of liquid sodium in a pool-type geometry. *International Journal of Heat and Mass Transfer*, 158:119968, 2020.

[8] Rebecca Rose Romatoski and Lin-Wen Hu. Fluoride salt coolant properties for nuclear reactor applications: A review. *Annals of Nuclear Energy*, 109:635–647, 2017.

[9] Roberto Serrano-López, Jordi Fradera, and Santiago Cuesta-López. Molten salts database for energy applications. *Chemical Engineering and Processing: Process Intensification*, 73: 87–102, 2013.

[10] Manohar S Sohal, Matthias A Ebner, Piyush Sabharwall, and Phil Sharpe. Engineering database of liquid salt thermophysical and thermochemical properties. Technical report, Idaho National Laboratory (INL), 2010.

[11] Karl Britsch, Mark Anderson, Paul Brooks, and Kumar Sridharan. Natural circulation flibe loop overview. *International Journal of Heat and Mass Transfer*, 134:970–983, 2019.

[12] AK Srivastava, Jayaraj Y Kudariyawar, A Borgohain, SS Jana, NK Maheshwari, and PK Vijayan. Experimental and theoretical studies on the natural circulation behavior of molten salt loop. *Applied Thermal Engineering*, 98:513–521, 2016.

[13] Liu Bin, Wu Yu-ting, Ma Chong-fang, Ye Meng, and Guo Hang. Turbulent convective heat transfer with molten salt in a circular pipe. *International communications in heat and mass transfer*, 36(9):912–916, 2009.

[14] Yu-Ting Wu, Cong Chen, Bin Liu, and Chong-Fang Ma. Investigation on forced convective heat transfer of molten salts in circular tubes. *International Communications in Heat and Mass Transfer*, 39(10):1550–1555, 2012.

[15] Ojasvin Arora, Blain Lancaster, Se Ro Yang, Rodolfo Vaghetto, and Yassin Hassan. Advanced flow and temperature measurements in a forced convection molten salt test loop. *Annals of Nuclear Energy*, 159:108269, 2021.

[16] David Eugene Holcomb, Roger A Kisner, and Sacit M Cetiner. Instrumentation framework for molten salt reactors. Technical report, Oak Ridge National Lab.(ORNL), Oak Ridge, TN (United States), 2018.

[17] Michael Andrew Pantano. *Investigation of performance of an ultrasonic flow meter for potential molten salt reactor applications*. PhD thesis, Massachusetts Institute of Technology, 2016.

[18] *Permanently installed ultrasonic flowmeter for liquids*. Flexim, 9 2019. 2-3.

[19] Abhisek Ukil, Hubert Braendle, and Peter Krippner. Distributed temperature sensing: review of technology and applications. *IEEE Sensors Journal*, 12(5):885–892, 2011.

[20] Stephen T Kreger, Nur Aida Abdul Rahim, Naman Garg, Sandra M Klute, Daniel R Metrey,

Noah Beaty, James W Jeans, and Robert Gamber. Optical frequency domain reflectometry: principles and applications in fiber optic sensing. In *Fiber Optic Sensors and Applications XIII*, volume 9852, page 98520T. International Society for Optics and Photonics, 2016.

[21] Zhenyang Ding, Chenhuan Wang, Kun Liu, Junfeng Jiang, Di Yang, Guanyi Pan, Zelin Pu, and Tiegen Liu. Distributed optical fiber sensors based on optical frequency domain reflectometry: A review. *Sensors*, 18(4):1072, 2018.

[22] *ODiSI 6000 Series Data Sheet*. Luna Innovations, 10 2020. pg. 3.

[23] Precision Rated Optics. Ofs-935c fusion splicer. URL `https://precisionratedoptics.com/shop/splicing/fusion-splicers/ofs-935c-fusion-splicer-core-alignment/`.

[24] *Buffer Removal Techniques for Optical Fiber*. Fiber Guide Industries, 11 2018. pg. 7 and 8.

[25] Jie Qiu, Bin Leng, Huajian Liu, Digby D Macdonald, Angjian Wu, Yanyan Jia, Wandong Xue, Guojun Yu, and Xingtai Zhou. Effect of so42- on the corrosion of 316l stainless steel in molten flinak salt. *Corrosion Science*, 144:224–229, 2018.

[26] NIST. Uncertainty for linear calibration using check standards. URL `https://www.itl.nist.gov/div898/handbook/mpc/section3/mpc3672.htm`.

[27] David Holler, Rodolfo Vaghetto, and Yassin Hassan. High-resolution wall temperature measurements with distributed fiber optic sensors. *International Journal of Thermal Sciences*, 145:106042, 2019.

[28] Stephen Lomperski, Craig Gerardi, and William David Pointer. Fiber optic distributed temperature sensor mapping of a jet-mixing flow field. *Experiments in Fluids*, 56(3):55, 2015.

APPENDIX A

A.1 ODTS Installation Configurations

A.1.1 Configuration 1

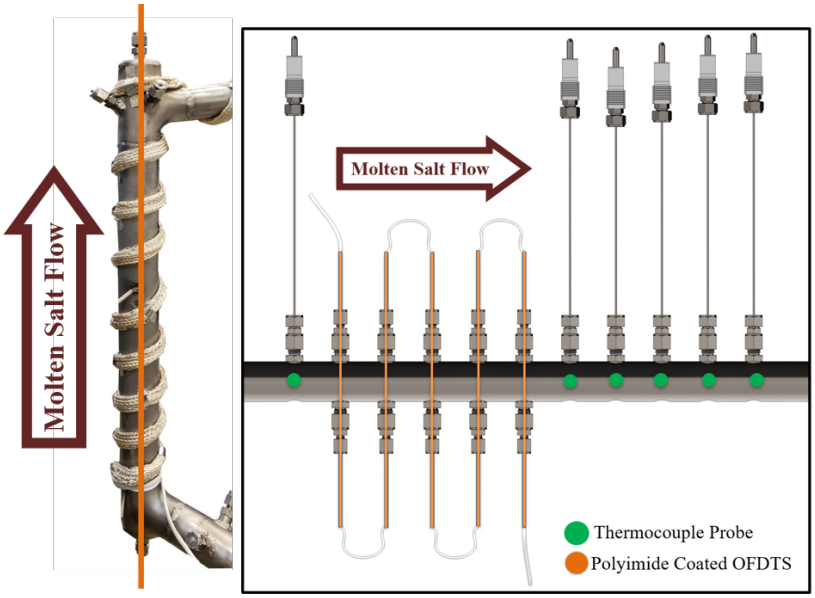

Figure A.1: First OFDTS Installation

A.1.2 Configuration 2

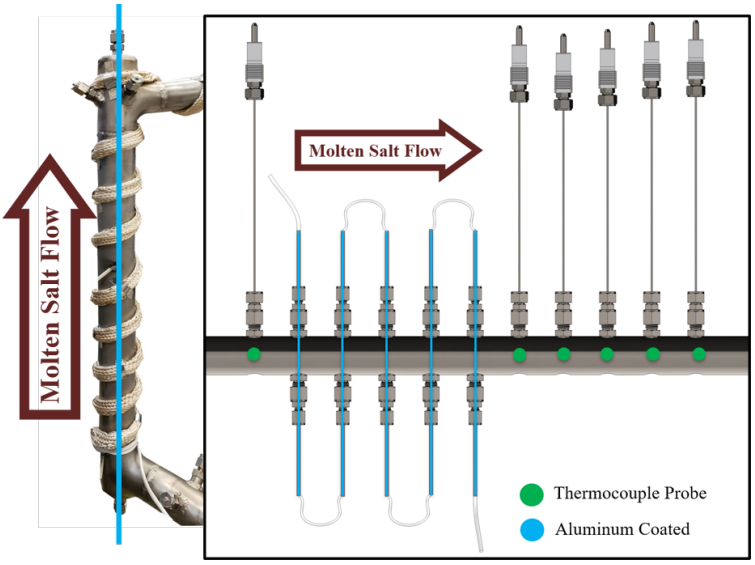

Figure A.2: Second OFDTS Installation

A.1.3 Configuration 3

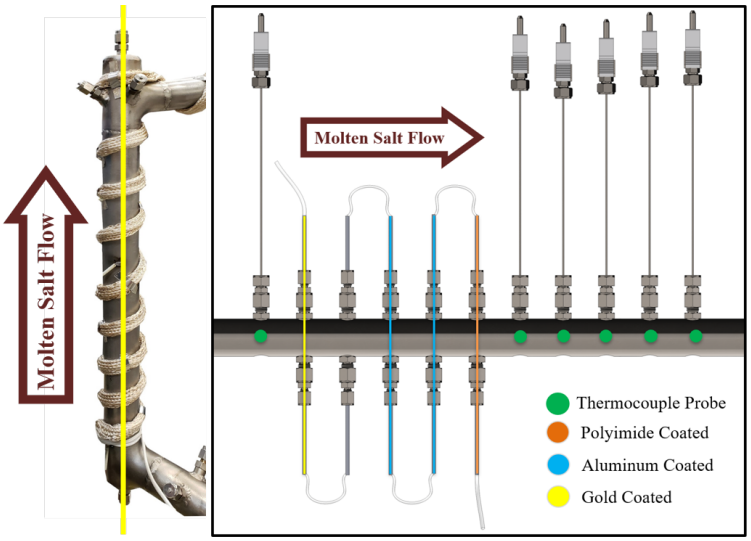

Figure A.3: Third OFDTS Installation